Fast Anisotropic Edge Detection Using Gamma Correction in Color Images

Baptiste Magnier, Philippe Montesinos, Daniel Diep

Fast Anisotropic Edge Detection Using Gamma Correction in Color Images

Baptiste Magnier, Philippe Montesinos and Daniel Diep
Ecole des Mines d'ALES, LGI2P, Parc Scientifique G.Besse 30035 Nimes Cedex 1
{Baptiste.Magnier,Philippe.Montesinos,Daniel.Diep}@mines-ales.fr

Abstract

In this paper we propose a new edge detector based on anisotropic linear filtering, local maximization and gamma correction. The novelty of this approach resides in the mixing of ideas coming both from directional recursive linear filtering and gamma correction. A peculiarity of our anisotropic edge detector is that it is based on the use of two elongated and oriented filters in two different directions. We show in this paper that unlike classical edge detection methods, gamma correction does not perturb the edge detection but enhances clearly the resulting contours obtained, especially in over-exposed or under-exposed areas of the image. Consequently, we propose a new edge operator enabling very precise detection of edge points involved in large structures. This detector has been tested successfully on various image types presenting difficult problems for classical edge detection methods.

1. Introduction

Edges detection methods differ in the types of smoothing filters that are applied, they also differ in the types of filters used for computing gradient estimates [1] [12] [5] [6] [9]. The work presented in this paper is motivated by applications needing a "good" edge detector [1], providing precise and really informative edge points with the fewest false detection rate as possible. For example, in the domain of object finding or recognition in natural scenes, objects may present various shapes and color aspects. For such cases, many local methods involving for example points of interest and color invariants fail.

In such applications, edge detection remains a central key point as it can provide geometrical information. In most cases, commonly used edge detectors [1] [12] [13] do not lead directly to object edges, then contours must be searched among numerous edge points. Furthermore, crossing edges and corners are not well detected with the methods of [1] and [12]. Indeed, the filtered value is greater near the corner as on the corner itself. Authors of [5] introduced steerable filters which can be tuned to a specific orientation by making a linear combination of isotropic filters. Edge detection techniques using anisotropic Gaussian filtering have been introduced in [10] and fast implemented in [6]. These approaches are able to correctly detect large linear structures. For anisotropic filtering methods like in [6] and [7], the robustness against noise depends strongly on the two smoothing parameters of the filter. If these parameters increase, the detection is less sensitive to noise, but small structures are considered as noise. Consequently, the precision of the detected edge points decreases strongly at corners points and for non straight object contour parts. In [9] is developped a new anisotropic edge detection method able to detect crossing edges and corners due to two elongated and oriented filters in two different directions.

In this paper a method for the precise detection of edge points belonging to large structures is described. Using gamma correction, we furthermore attempt to detect edges in parts of an image where objects may be over- or under-exposed. This method involves anisotropic filtering [9] [8] and gamma curves [11] to extract contours of objects just by image differentiation. Our approach precisely detects corners and crossing edges thanks to two specific Gaussian oriented kernels in two different directions. Edges are computed on three images: the original image and two gamma-corrected images. Our edge detector involves directional linear filtering by means of recursive filters followed by the computation of an edge operator built with a local directional maximization of the response of the filters.

In the section 2, we first recall the basics of anisotropic edge detection. We present a robust edge detector in the section 3. Then, we describe gamma correction in section 4 and present our edge detector on gray-scale and color images. We evaluate quantitatively and compare our method with other approaches in section 5. The section 6 is devoted to experimental results and comparison with other methods. Finally, the section 7 concludes this paper.

2 Anisotropic Edge Detection

Anisotropic edge detection can be seen as a generalization of color edge detection. Suppose that the image is smoothed with a bank of rotated anisotropic Gaussian kernels:

$$g_{(\mu,\lambda)}(x,y,\theta) = C.e^{-\begin{pmatrix} x & y \end{pmatrix} R_\theta^{-1} \begin{pmatrix} \frac{1}{2\,\mu^2} & 0 \\ 0 & \frac{1}{2\lambda^2} \end{pmatrix} R_\theta \begin{pmatrix} x \\ y \end{pmatrix}} \quad (1)$$

where C is a normalization coefficient, R_θ a rotation matrix of angle θ, (x, y) the coordinates of the pixel and (μ,

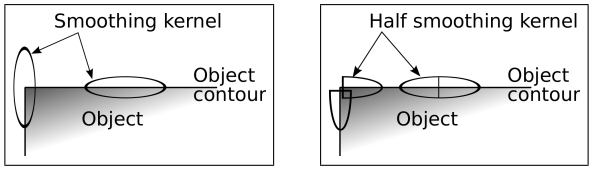

(a) (b)

Figure 1. (a) Full and (b) Half Anisotropic Gaussian kernels at linear portions of contours and at corners.

λ) are the two standard-deviations of the Gaussian filter. By convolution of the image I with these rotated kernels, we obtain a collection of smoothed images I_θ which can be derived along X and Y axis to obtain anisotropic directional derivatives $I_{\theta X}$ and $I_{\theta Y}$. These derivatives can now be combined in an orientation tensor [6]. Then, gradient is computed with the largest eigenvalue of the tensor.

3 An Anisotropic Edge Detector Using Half Smoothing Kernels

As pointed out in section 1, the anisotropic edge detector described in section 2 performs well at linear portions of contours (kernels are illustrated in Fig. 1), but near corners, the gradient magnitude decreases as the edge information under the scope of the filter decreases (Fig. 8 and 10 (h) illustrate this problem). Consequently, the robustness to noise decreases when the two smoothing parameters decrease whereas small objects are considered as noise if these parameters increase.

The simplest solution to bypass this effect is to consider paths crossing each pixel in several directions. The idea developed in [9] and [8] is to "cut" the derivative (and smoothing) kernel into two parts, i.e. two directions (see Fig. 2). As we need only the causal part of the filter, the operation corresponds to the Heaviside function H. Smoothing the image with a "cut" kernel by the middle is equivalent to smooth the image with a bank of rotated "half" anisotropic Gaussians:

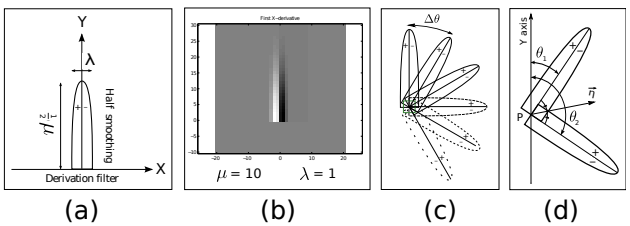

(a) (b) (c) (d)

Figure 2. Rotating filter: (a) Edge operator (*derivation filter on X and half smoothing filter on Y*). (b) Example of a discretized filter. (c) Rotated filters with an angle of $\Delta\theta$. (d) Computation of $\eta(x, y)$ from θ_1 and θ_2.

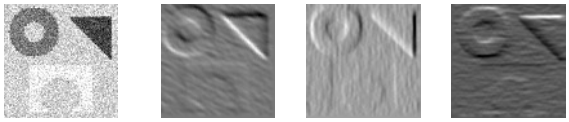

(a) 128×128 (b) θ=120 (c) θ=180 (d) θ=270

Figure 3. Image and its normalized derivatives at different orientations θ with $\mu = 5$ and $\lambda = 1$.

$$G_{(\mu,\lambda)}(x, y, \theta) = H\left(R_\theta \begin{pmatrix} x \\ y \end{pmatrix}\right) g_{(\mu,\lambda)}(x, y, \theta). \quad (2)$$

By convolution with these rotated kernels (see Fig. 2(b)), we obtain a collection of directionally smoothed and derivated images $I_\theta = I * G_{(\mu,\lambda)}(\theta)$.

For computational efficiency, we proceed in a first step to the rotation of the image at some discretized orientations from 0 to 360 degrees (of $\Delta\theta = 1$, 2, 5, or 10 degrees, depending on the angular precision needed and the smoothing parameters) before applying non rotated derivative smoothing filters. As the image is rotated instead of the filters, the filtering implementation can use an efficient recursive approximation of the Gaussian filter [2]. As presented in [9], the implementation is quite straightforward. In a second step, we apply an inverse rotation of the smoothed image and obtain a bank of $360/\Delta\theta$ images (some examples of derivated images are shown in Fig. 3).

At each pixel of coordinates (x, y), a derivation filter is applied to obtain a derivative information called $\mathcal{Q}(x, y, \theta)$:

$$\mathcal{Q}(x, y, \theta) = I_\theta * C_1.H(-y)\, x\, e^{-\left(\frac{x^2}{2\lambda^2} + \frac{y^2}{2\mu^2}\right)} \quad (3)$$

where I_θ corresponds to a rotated image of orientation θ and C_1 to a normalization coefficient. $\mathcal{Q}(x, y, \theta)$ represents a quality measure of a line issued from a pixel in the direction θ. This measure is an integration of the slope of the image function in this perpendicular direction. Some examples of $\mathcal{Q}(x, y, \theta)$ are shown on a selection of different point types in Fig. 5. In the direction of the contour, "half smoothing" is performed. Now, the edge detection problem becomes an optimization problem.

For obtaining a gradient $\|\nabla I\|$ and its associated direction η on each pixel P, we first compute local extrema of the

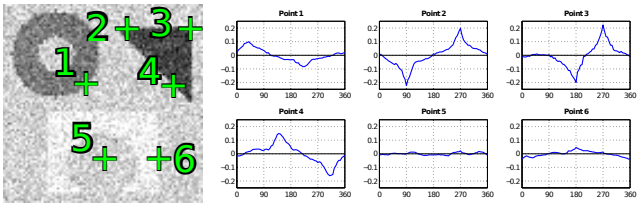

Figure 5. Points selection on image in Fig. 3(a) and its associated $\mathcal{Q}(x, y, \theta)$ with $\Delta\theta = 5°$.

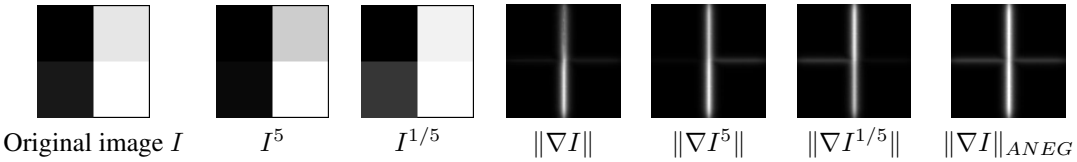

Figure 4. Principle of the ANEG: computation of a gradient on the 3 images I, I^γ, $I^{1/\gamma}$ and selection of the highest gradient value called $\|\nabla I\|_{ANEG}$.

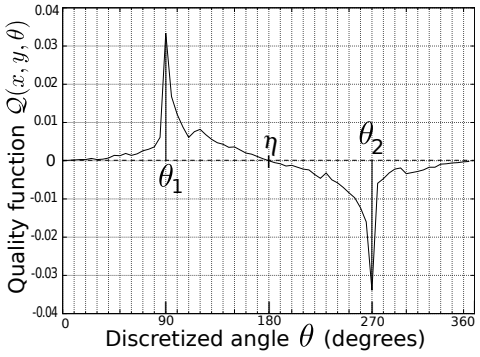

Figure 6. Example of a function $\mathcal{Q}(x, y, \theta)$.

function $\mathcal{Q}(x, y, \theta)$, θ_1 and θ_2 (illustrated in Fig. 6). θ_1 and θ_2 define a curve crossing the pixel (an entering and leaving path). Then two of these local extrema are combined to maximize $\|\nabla I\|$:

$$\theta_1 = \underset{\theta\in[0,360[}{\arg\max}\,(\mathcal{Q}(x,y,\theta)), \tag{4}$$

$$\theta_2 = \underset{\theta\in[0,360[}{\arg\min}\,(\mathcal{Q}(x,y,\theta)), \tag{5}$$

$$\|\nabla I\| = \mathcal{Q}(x,y,\theta_1) - \mathcal{Q}(x,y,\theta_2). \tag{6}$$

Then we simply estimate η (see Fig. 2(c) and 6 (a)) by the mean value of θ_1 and θ_2: $\eta = (\theta_1 + \theta_2)/2$

$\|\nabla I\|$ and η once obtained, edges can easily be extracted by computing local maxima of $\|\nabla I\|$ in the direction η followed by an hysteresis threshold (Fig. 2(c)).

4 An Anisotropic Edge Detector Using Gamma Correction (ANEG)

Let us note τ_L the hysteresis lower threshold and τ_H the higher. σ corresponds to the standard-deviations of the Gaussian filter in [1], α to the width of the smoothing parameter in [12] and r to the radius of the nucleus in [13].

In order to detect edges inside over or under-exposed areas of the image, τ_L and τ_H must be very small. But computing contours with low threshold parameters may create undesired contours in other parts of the image (see Fig. 8). For that reason, we have developed a new edge detector using gamma correction able to compute over and under-exposed object edges without generating false contours inside objects or textures.

4.1 Gamma Correction

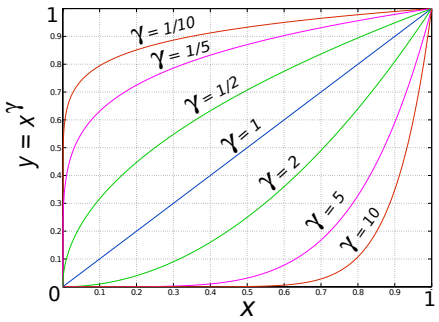

Figure 7. Gamma curves where X represents the normalized pixel intensity.

Gamma correction is the name of a nonlinear operation which modifies pixel intensities in an image [11]. Indeed, in the case of an over-exposed image, gamma correction can be used to darken this image and conversely for an under-exposed image, it can lead to brighter images. Similar ideas are used in high dynamic range images [4] but not in edge detection. Gamma correction is defined as follows:

$$I_{out}(P) = (I(P))^\gamma,\ \gamma > 0 \text{ and } I(P) \in [0,1]\,, \tag{7}$$

where $I(P)$ and $I_{out}(P)$ are respectively the input and output normalized pixel intensites. Fig. 7 shows the behavior of the gamma curve in function of different values of γ. $\gamma > 1$ leads to a darker image whereas $\gamma < 1$ leads to a brighter image (an example of gamma correction on an image is presented on Fig. 4).

4.2 Edge Detection Using Gamma Correction

Fig. 4 presents the edge detection problem without gamma correction. Indeed, gradient result $\|\nabla I\|$ obtained in the image in Fig. 4 shows that the vertical gradients are stronger than the horizontal ones. However, with the gamma correction, the horizontal contour becomes brighter (Fig. 4). In order to solve this problem, we propose a new anisotropic edge detector using gamma correction (ANEG).

The solution is to compute a gradient with the method presented in section 3 on the three following images: I, I^γ and $I^{1/\gamma}$ and then to combine these three informations obtained. I represents the original image in gray level, I^γ

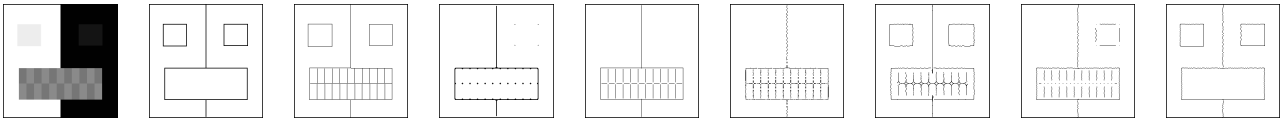

Original 300×300	Desired contours: two squares over and under-exposed plus the grey rectangle	Laplacian mask 3×3	SUSAN [13] $r=3$ $\tau_L=0.01$ $\tau_H=0.01$	Shen-Castan [12] $\alpha=1$ $\tau_L=0.03$ $\tau_H=0.035$	Canny [1] $\sigma=1$ $\tau_L=0.028$ $\tau_H=0.0285$	Anisotropic Gaussian [6] $\mu=5, \lambda=1$ $\tau_L=0.01$ $\tau_H=0.05$	Half kernels [9] $\mu=5, \lambda=1$ $\tau_L=0.01$ $\tau_H=0.06$	ANEG $\mu=5, \lambda=1$ $\tau_L=0.1$ $\tau_H=0.1$

Figure 8. Different edge detection methods on a particular synthetic image.

represents I corrected with the parameter γ and $I^{1/\gamma}$ is I corrected with the parameter $1/\gamma$ ($\gamma > 1$). These three images I, I^γ and $I^{1/\gamma}$ are considered separately as three gray-scale images. Then, we select the highest gradient value $\|\nabla I\|_{ANEG}$ (example in Fig. 4). We can combine them into the following formulas:

$$\|\nabla I\|_{ANEG} = \max(\|\nabla I\|, \|\nabla I^\gamma\|, \|\nabla I^{1/\gamma}\|). \quad (8)$$

In Fig. 9(b), the pixel belongs to an edge of an object which can be considered as over-exposed, so from eq. 3, 4, 5, 6 and 8, $\|\nabla I\|_{ANEG} = \|\nabla I^5\|$. However, in the presence of noise, $\|\nabla I\|_{ANEG}$ is not modified because contrary to a pixel belonging to an edge (Fig. 9(b)), the local extrema of $\mathcal{Q}(x, y, \theta)$ are not so high (see Fig. 9(a)).

After this step, edges are extracted by computing local maxima of $\|\nabla I\|_{ANEG}$ in the direction η_{ANEG}:

$$\eta_{ANEG} = \underset{\eta_I, \eta_{I^\gamma}, \eta_{I^{1/\gamma}}}{\arg\max} \left(\|\nabla I\|, \|\nabla I^\gamma\|, \|\nabla I^{1/\gamma}\|\right). \quad (9)$$

4.3 Adaptation to Color Images

A color image $\mathbf{I}$ is composed of three image planes: red, green and blue (R, G and B). The structure tensor in [3] enables an extension of classical edge detection [1] [12] on vector images. Similarly, anisotropic edge detection in [6] has also been extended to color using a tensor in [7].

The anisotropic edge detector described in section 3 can be applied on gray-scale images, but it can also be adapted separately to the three planes of a color image as three gray-scale images. Indeed, as this filter does not compute derivative images along x and y direction, we do not need any tensor [3] to extend the edge detector to color images. Thus, we calculate the highest gradient value $\|\nabla \mathbf{I}\|$ using $\max$ which is the favouring norm to color :

$$\|\nabla \mathbf{I}\| = \max(\|\nabla R\|, \|\nabla G\|, \|\nabla B\|), \quad (10)$$

$$\eta_{\mathbf{I}} = \underset{\eta_R, \eta_G, \eta_B}{\arg\max} \left(\|\nabla R\|, \|\nabla G\|, \|\nabla B\|\right). \quad (11)$$

After this step, edges can easily be extracted by computing local maxima of $\|\nabla \mathbf{I}\|$ in the η direction.

Gamma correction can be applied on a color image, we use the gamma correction on the three image channels R, G and B. From these three planes, we obtain three groups of three images: $\mathbf{I}$, $\mathbf{I}^\gamma$ and $\mathbf{I}^{1/\gamma}$. Thus, from eq. (11) and (12):

$$\|\nabla \mathbf{I}^\gamma\| = \max(\|\nabla R^\gamma\|, \|\nabla G^\gamma\|, \|\nabla B^\gamma\|), \quad (12)$$

$$\|\nabla \mathbf{I}^{1/\gamma}\| = \max(\|\nabla R^{1/\gamma}\|, \|\nabla G^{1/\gamma}\|, \|\nabla B^{1/\gamma}\|), \quad (13)$$

$$\eta_{\mathbf{I}^\gamma} = \underset{\eta_{R^\gamma}, \eta_{G^\gamma}, \eta_{B^\gamma}}{\arg\max} \left(\|\nabla R^\gamma\|, \|\nabla G^\gamma\|, \|\nabla B^\gamma\|\right),$$

$$\eta_{\mathbf{I}^{1/\gamma}} = \underset{\eta_{R^{1/\gamma}}, \eta_{G^{1/\gamma}}, \eta_{B^{1/\gamma}}}{\arg\max} \left(\|\nabla R^{1/\gamma}\|, \|\nabla G^{1/\gamma}\|, \|\nabla B^{1/\gamma}\|\right).$$

Finally, from previous equations and eq. (2), we obtain:

$$\|\nabla \mathbf{I}\|_{ANEG} = \max(\|\nabla \mathbf{I}\|, \|\nabla \mathbf{I}^\gamma\|, \|\nabla \mathbf{I}^{1/\gamma}\|), \quad (14)$$

$$\eta_{ANEG} = \underset{\eta_{\mathbf{I}}, \eta_{\mathbf{I}^\gamma}, \eta_{\mathbf{I}^{1/\gamma}}}{\arg\max} \left(\|\nabla \mathbf{I}\|, \|\nabla \mathbf{I}^\gamma\|, \|\nabla \mathbf{I}^{1/\gamma}\|\right).$$

Now, edges using gamma correction are extracted by computing local maxima of $\|\nabla \mathbf{I}\|_{ANEG}$ in the direction η_{ANEG} followed by an hysteresis threshold.

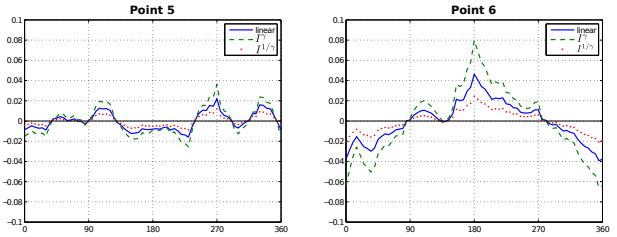

(a) Point inside a homogeneous noisy region

(b) Point belonging to a contour of an over-exposed and noisy object

Figure 9. $\mathcal{Q}(x, y, \theta)$ function using gamma correction (γ=5) of points 5 and 6 of the noisy image in Fig. 5. $\mu=5$, $\lambda=1$ and $\Delta\theta=5^o$.

5 Quantitative Evaluation

In order to carry out some quantitative results, we have conducted a number of tests with synthetic images including a black square (Fig. 10). In our test, we performed edge detection and compared the result to the original image, pixel per pixel. We thus obtained a quantified error by making the difference between the two images. We analyzed the effect of adding a uniform white noise on the original image using the following formula: $I_m = (1 - L)I_0 + L.I_N$, where I_0 is the original image, I_N an image of random uniform noise and I_m the resulting noisy image. As expected, the number of errors increases monotonically with the noise level L. Curves plotted on Fig. 11 represent (a) the number of true negative pixels, i.e. undetected edges points, and (b) the number of false positive pixels, i.e. unexisting contour

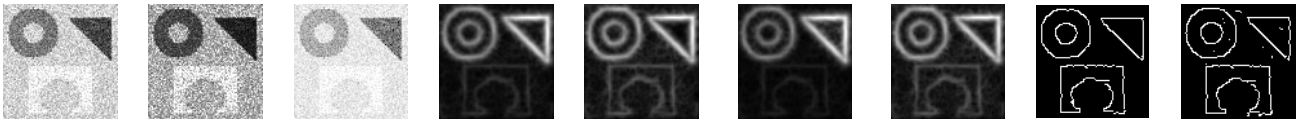

(a) I (b) I^5 (c) $I^{1/5}$ (d) $\|\nabla I\|$ (e) $\|\nabla I^5\|$ (f) $\|\nabla I^{1/5}\|$ (g) (h) (i)

Figure 12. Result of the ANEG detector with $\mu = 5$, $\lambda = 1$ (a) Original image I 128×128, (g) $\|\nabla I\|_{ANEG}$. (h) ANEG with $\tau_L = 0.15$ and $\tau_H = 0.2$. (i) Result of [9] (i.e. edges on (a)), $\tau_L = 0.08$ and $\tau_H = 0.1$.

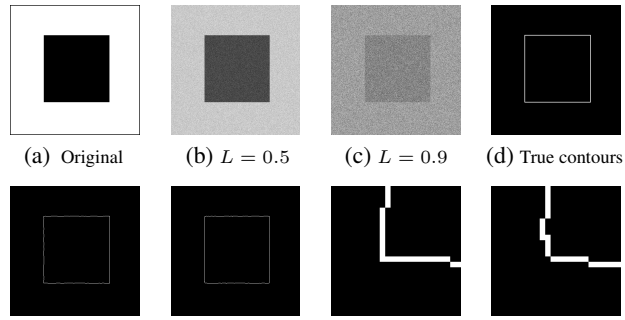

(a) Original (b) $L = 0.5$ (c) $L = 0.9$ (d) True contours

(e) ANEG on the image in (b) (f) [6] on the image in (b) (g) Detail of corner detected by ANEG (h) Detail of corner detected by [6]

Figure 10. Images 400×400 with different levels of noise L and comparison with [6]. For (e), (f), (g) and (h): $\mu = 10$, $\lambda = 1$ and $\Delta\theta = 5^o$.

points, which both constitute errors. Fig. 11(c) and (d) show magnified details of (a) and (b). For each approach, we have also computed the number of correctly detected corners in Fig. 11(e) among the 4 corners of the square presented in Fig. 10(a). Compared to Canny [1] and Shen-Castan [12] approaches, the three anisotropic edge detection methods (Gaussian anisotropic [6], Half Kernels [9] and ANEG) perform well and show a good robustness to noise. However, Half Kernels and ANEG methods are better than Gaussian anisotropic at detecting corners (see details of zoomed corners on Fig. 10(g) and (h)).

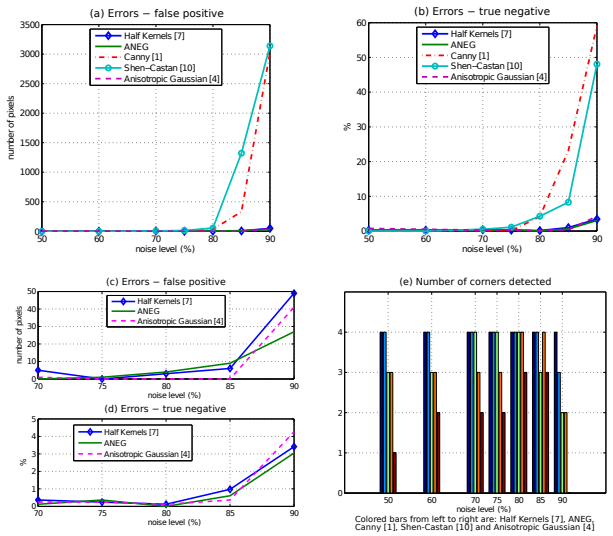

Figure 11. Influence of noise level on different edge detection methods.

In conclusion, Half Kernels and ANEG provide satisfying results, even in presence of high noise. This evaluation has been made on a synthetic image, allowing us to provide quantitative results, provided that actual contours are known with a one-pixel precision. In the next section, we show that similar results are obtained on real images.

6 Experimental Results

In our results, $\Delta\theta = 5°$ for all anisotropic filters ([6] [7] [9] and ANEG). In the vectorial case, we use the same parameters μ and λ for each channel of the image and each corrected image. The γ (and respectively $1/\gamma$) parameter is the same for each channel of the image. γ=5 is sufficient to detect edges in over- or under-exposed areas of images. Thresholds τ_L and τ_H are chosen in function of a maximum of desired contours and a minimum of undesired contours. The choice of the parameters μ and λ is to be done in function of the size of the original image and the size of contours that we want to detect. Actually, if we need small details or contours in a small image, μ should be small (for example μ=5), whereas, for long structures, μ should be larger (for example μ=10). For its part, parameter λ corresponds to the width of the filter and does not need to be very large because it is linked to the desired precision on the edge.

The first result on a gray-scale image is presented in Fig. 12, the parameters of the half smoothing kernel are $\mu = 5$ and $\lambda = 1$. The result of our detector is less noisy than the result of [9] and contours are more regular. So the $ANEG$ detector appears to be more robust to noise than [9]. Moreover, our result is more precise and continuous than [1] [12] and [6] (Fig. 13(a) (b) (c)). Fig. 13(c) and (e) show that gamma correction followed by eq. 2 is not adapted for edge detection with isotropic [1] and anisotropic filter of [6].

In results presented in Fig. 14(e), edges are more con-

(a) [1] $\sigma = 1$ $\tau_L = 0.01$ $\tau_H = 0.8$ (b) [12] $\alpha = 1$ $\tau_L = 0.05$ $\tau_H = 0.08$ (c) [6] $\tau_L = 0.1$ $\tau_H = 0.22$ (d) [1] $\sigma = 1$ $\tau_L = 0.05$ $\tau_H = 0.12$ (e) [6] $\tau_L = 0.01$ $\tau_H = 0.03$

Figure 13. Results issued from Fig.12(a). For (c) and (e): $\mu = 5$, $\lambda = 1$ and $\Delta\theta = 5°$. Gamma correction in (d) and (e).

(a) Peppers original 266×266

(b) [1] $\sigma = 1$ $\tau_L = 0.001$, $\tau_H = 0.01$

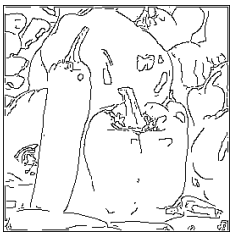

(c) [12] $\alpha = 1$ $\tau_L = 0.04$, $\tau_H = 0.05$

(d) [9] $\mu = 5$, $\lambda = 1$ $\tau_L = 0.01$, $\tau_H = 0.2$

(e) ANEG $\mu = 5$, $\lambda = 1$ $\tau_L = 0.01$, $\tau_H = 0.25$

(f) Original color image 321×165

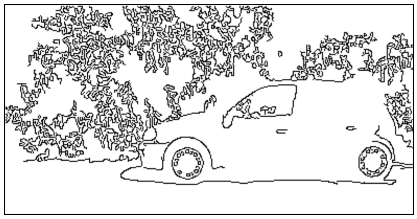

(g) [1], $\sigma = 1$, $\tau_L = 0.001$, $\tau_H = 0.1$

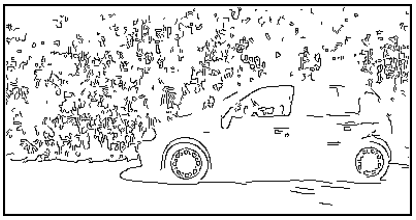

(h) [12], $\alpha = 1$, $\tau_L = 0.1$, $\tau_H = 0.15$

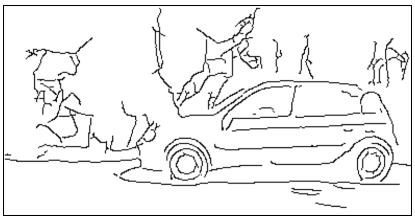

(i) [7], $\tau_L = 0.01$, $\tau_H = 0.3$

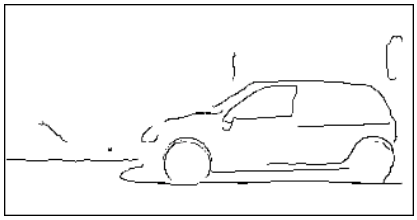

(j) [9], $\tau_L = 0.01$, $\tau_H = 0.5$

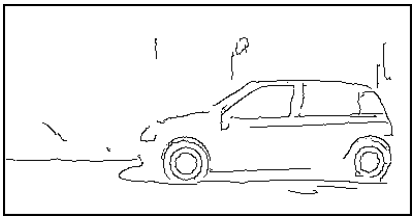

(k) ANEG, $\tau_L = 0.3$, $\tau_H = 0.4$

Figure 14. Result on natural color images. For (i), (j) and (k): $\mu = 10$, $\lambda = 1$.

tinuous than in Fig. 14(b), (c) and (d), especially the green pepper in the middle which is correctly detected.

In the last image, Fig. 14(f), classical [1] [12] and anisotropic Gaussian edge detection [7] fails to detect the car because their results are perturbed by the texture. The result of [9] is better but the ANEG brings more details in over- and under-exposed parts of the car (especially wheels) without creating false edges inside the texture.

Somme results on different images are available online.[1]

7 CONCLUSION

We have proposed in this paper an anisotropic edge detector using gamma correction in color images. This detector is formed by two half rotating smoothing kernels. Due to its strong smoothing in the directions of the edges, the detection is not sensitive to noise. Moreover, it stays localized at the level of the edges because of its small smoothing in the perpendicular direction of the contours. As a result, Gamma correction does not introduce false edges detections but it enables to find edges in parts of the image where objects are over-exposed or under-exposed. Finally, this edge detector performs fine at corners, so next on our agenda is to extend this method to corners and junctions detection using the two directions of the kernels. Potential applications are camera calibration and interest points matching.

[1] www.lgi2p.ema.fr/~magnier/Research/ANEG/Demos

References

[1] F. Canny, "A computational approach to edge detection", *IEEE TPAMI*, 8(6), 1986, pp. 679–698.

[2] R. Deriche, "Recursively implementing the gaussian and its derivatives", In *ICIP*, pp. 263–267, 1992.

[3] S. Di Zenzo, "A note on the gradient of a multi-image", *CVGIP*, 33(1), 1986, pp. 116–125.

[4] R. Fattal, D. Lischinski, and M. Werman, "Gradient domain high dynamic range compression", *ACM Transactions on Graphics*, 21(3), 2002, pp. 249–256.

[5] W. T. Freeman and E. H. Adelson, "The design and use of steerable filters", *IEEE TPAMI*, 13, 1991, pp. 891–906.

[6] J. Geusebroek, A. Smeulders, and J. Van De Weijer, "Fast anisotropic gauss filtering", *ECCV 2002*, 2002, pp. 99–112.

[7] D. Knossow, J. Van De Weijer, R. Horaud, and R. Ronfard, "Articulated-Body Tracking Through Anisotropic Edge Detection", *Dynamical Vision*, 2007, pp. 86–99.

[8] B. Magnier, P. Montesinos, and D. Diep, "Texture Removal by Pixel Classification using a Rotating Filter", In *IEEE ICASSP*, pp. 1097–1100, 2011.

[9] P. Montesinos and B. Magnier, "A New Perceptual Edge Detector in Color Images", In *ACIVS*, pp. 209–220, 2010.

[10] P. Perona, "Steerable-scalable kernels for edge detection and junction analysis", *IMAVIS*, 10(10), 1992, pp. 663–672.

[11] C. Poynton, *A technical introduction to digital video*, John Wiley & Sons, Inc. New York, NY, USA, 1996.

[12] J. Shen and S. Castan, "An optimal linear operator for step edge detection", *CVGIP*, 54(2), 1992, pp. 112–133.

[13] S. Smith and J. Brady, "SUSAN A new approach to low level image processing", *IJCV*, 23(1), 1997, pp. 45–78.